PCCP

Accepted Manuscript

This is an *Accepted Manuscript*, which has been through the Royal Society of Chemistry peer review process and has been accepted for publication.

Accepted Manuscripts are published online shortly after acceptance, before technical editing, formatting and proof reading. Using this free service, authors can make their results available to the community, in citable form, before we publish the edited article. We will replace this *Accepted Manuscript* with the edited and formatted *Advance Article* as soon as it is available.

You can find more information about *Accepted Manuscripts* in the Information for Authors.

Please note that technical editing may introduce minor changes to the text and/or graphics, which may alter content. The journal's standard Terms & Conditions and the Ethical guidelines still apply. In no event shall the Royal Society of Chemistry be held responsible for any errors or omissions in this *Accepted Manuscript* or any consequences arising from the use of any information it contains.

ROYAL SOCIETY OF CHEMISTRY

www.rsc.org/pccp

Physical Chemistry Chemical Physics Accepted Manuscript

Towards High Refrigeration Capability: The Controllable Structure of Hierarchical $Bi_{0.5}Sb_{1.5}Te_3$ Flakes on a Metal Electrode

Lili Cao[1], Yuan Deng[1,*], Hongli Gao[1], Yao Wang[1], Xin Chen[2], Zhixiang Zhu[2]

[1]Beijing Key Laboratory of Special Functional Materials and Films, School of Materials Science & Engineering, Beihang University, Beijing, 100191, China

[2]Department of New Electrical Materials and Microelectronics, State Grid Smart Grid Research Institute, Beijing, 102211, China

ABSTRACT: The refrigeration capability of a thermoelectric device is dictated by interfacial effects and the figure of merit ZT, which govern the contact resistance and the Carnot efficiency for heat conversion. Here we report a controllable (110) oriented $Bi_{0.5}Sb_{1.5}Te_3$ film growing on a Cu film electrode. The hierarchical $Bi_{0.5}Sb_{1.5}Te_3$ film is composed of tens of cactus like flakes that have a (110) oriented back bone and abundant 50 _ 80 nm branches in the (015) direction. The lattice mismatch of the (110) oriented $Bi_{0.5}Sb_{1.5}Te_3$ to the Cu electrode is estimated to be appoximately 2.4%, which implies a decreased interfacial dislocation density and formation of fewer interfacial defects leading to low contact resistance (1.0×10^{-9} Ω m^2). The enhanced out plane ZT ≈ 0.73 is calculated from the in plane properties. Hence a maximum heat-flux pumping capability of 138 W cm^{-2} can be obtained for T_c = 400 K and the corresponding temperature difference is 6 K. Our work indicates that the control of the metal-semiconductor interfacial structure is an efficient approach to improve the refrigeration capability.

KEYWORDS: thermoelectric refrigeration, contact resistance, thin film, $Bi_{0.5}Sb_{1.5}Te_3$, interface

Physical Chemistry Chemical Physics Accepted Manuscript

Physical Chemistry Chemical Physics Accepted Manuscript

INTRODUCTION

Thermoelectric coolers (TECs) are recognized for transferring heat from one side of the device to the other. The consumption of electrical energy depends on the direction of the current, by means of the Peltier effect. TECs have many attractive features compared with other methods of refrigeration, such as long life, no moving parts, no emissions of toxic gases, low maintenance, and high reliability[1, 2]. TEC has great potential for the cooling of high heat fluxes, which is a crucial requirement for microelectronics. The maximum heat-flux pumping capability of TEC can be expressed as[3],

$$\frac{Q_{\max}}{S} = \frac{1}{L}\left[\frac{\alpha^2 T_c^2}{\left(\frac{2}{\sigma} + \frac{4r_c}{L}\right)} - k\Delta T\right] \quad (1)$$

Where Q, S, α, σ, κ, r_c, T_c and L are the cooling capacity, area, the Seebeck coefficient, electrical conductivity, thermal conductivity, contact resistivity, cold-side temperature and thickness of the materials, respectively.

To obtain a high heat-flux pumping capability, the figure of merit ($ZT = S^2\sigma T/\kappa$) needs to be maximized, and the thickness (L) and contact resistivity (r_c) need to be minimized. In the past decades, significant advancements have been achieved for the increase of ZT, because of developments in field of nanotechnology. An increase in ZT enhances phonon scattering at the boundaries to reduce the lattice thermal conductivity. Among the various classes of TE materials at room temperature, Bi_2Te_3 and related solid solutions still dominate commercial applications[4, 5]. $Bi_{0.5}Sb_{1.5}Te_3$ is the best-known p-type material for room-temperature refrigeration[6]. Nano-structured Bi_2Te_3-based materials, such as thin films[7], thick films[8, 9], and nanoscale inclusions in bulk materials[10],

Physical Chemistry Chemical Physics Accepted Manuscript

can be fabricated by methods such as metal-organic chemical vapor deposition (MOCVD) [11], molecular beem epitaxy (MBE)[12], ion track lithography[13], flash evaporation (FE)[14], spark plasma sintering (SPS)[15] and hot pressing[16]. Furthermore, the ZT value can be enhanced by controlling the preferential direction. The layered rhombohedral crystal structure of Bi_2Te_3 based materials drives the anisotropic thermal and electronic transport properties. This, indicates that the performance of Bi_2Te_3 based materials can be enhanced by controlling the preferential direction. For example, Zhao's group found that SnSe with a layered structure has a *ZT* of = 2.62 along the *b* axis and 2.3 along the *c* axis, and a significantly lower value of 0.8 along the *a* direction[17]. Chen and his colleagues maintained that further improvement in ZT could be achieved by the promotion of great *ab* reorientation of $Bi_2Te_{2.7}Se_{0.3}$ into the disk plane[18]. If the *ab* plane is perpendicular to the substrate in thin film, its out plane ZT will be significantly improved.

Moreover, equation (1) also shows that the heat-flux pumping capability increases with the decreasing thickness of thermoelectric materials, which indicates that thin film materials have a greater heat-flux pumping capability than bulk materials. Continuous efforts are invested towards controlling the interface scattering of bulk materials[19-21]. Furthermore, the influence of thermal and electrical contacts can no longer be neglected in series devices of small dimensions. As shown in Ref. 22, good metal-semiconductor contact (close to $1{\sim}10 \times 10^{-6}\ \Omega\ cm^2$) in thin films is a crucial requirement for thin film thermoelectric devices[3, 22]. However, the contact resistance of metal-semiconductor has been reported to be typically between 10^{-8} and $10^{-9}\ \Omega\ cm^2$ in thermoelectric devices[23]. It is difficult to control the interfacial structure in order to obtain a low contact resistance in thin films[24]. As it is mentioned in Ref. 25, the contact resistance is affected by factors

such as defects, impurities, or variation in the crystal size and orientation, and the formation of oxides or secondary phases at the interface between two different materials[25]. The lattice mismatching of the materials generate strains between layers, causing the dislocation of atoms and the formation of defects[24]. Hence, it is advantageous to deposit thermoelectric film on Cu thin films and to control lattice matching at the metal-semiconductor interface.

In this work, we fabricated a hierarchical (110) oriented p-type $Bi_{0.5}Sb_{1.5}Te_3$ thin film on copper thin film via a facile and low cost method: the magnetron sputtering method. In this process, the thermoelectric thin film was fabricated at a low temperature to achieve a simple and user friendly preparation process. The possible crystal growth mechanism of the $Bi_{0.5}Sb_{1.5}Te_3$ thin film was also discussed and the transport properties of the hierarchical thin films were investigated.

EXPERIMENTAL DETAILS

The $Bi_{0.5}Sb_{1.5}Te_3$ thin films were deposited on polished aluminum nitride (AlN)/ Polyimide (PI)/ Cu thin film substrate in Ar (flow rate at 25 sccm) at certain temperature by direct current sputtering method using a magnetron sputtering system (JGP-450a, SKY Technology Development Co., Ltd. Chinese Academy of Sciences). Before deposition the substrate was cleaned in turn using acetone, alcohol and de-ionized water for 15 min respectively in an ultrasonic bath. Commercial 60 mm diameter hot-pressed Cu and Ni target (99.99%) (Purchased from General Research Institute for Nonferrous Metals, China) was used and the distance between targets and substrates maintained at 90 mm. The Cu and Ni film was deposited at 200 $^{\circ}$C, 1.5 Pa, 30 W, and their deposition time were 2 h and 20 min respectively. Cu and Ni target was connected to a direct current

Physical Chemistry Chemical Physics Accepted Manuscript

Physical Chemistry Chemical Physics Accepted Manuscript

power supplier. At last, commercial 60 mm diameter hot-pressed $Bi_{0.5}Sb_{1.5}Te_3$ target (99.99%) (Purchased from General Research Institute for Nonferrous Metals, China) was used and the distance between targets and substrates maintained at 90 mm. The $Bi_{0.5}Sb_{1.5}Te_3$ film was deposited at 100-300 °C, 1.0 Pa, 30 W and 40 min-3 h. $Bi_{0.5}Sb_{1.5}Te_3$ target was connected to a direct current power supplier. After deposition, in-situ annealing was carried out in Ar atmosphere for 40 min.

The phase structures were investigated by X-ray diffraction (XRD) on a Rigaku D/MAX 2200 PC automatic X-ray diffractometer with Cu Kα radiation (λ=0.154056 nm), with operation voltage at 40 kV and current maintained at 40 mA. The $Bi_{0.5}Sb_{1.5}Te_3$ film was characterized with the aid of a high-resolution transmission electron microscope (HR-TEM) (JEOL JEM2100F).The morphology and composition of the thin films were observed on a field emission scanning electron microscopy (FE-SEM) (FEI Sirion 200) equipped with energy dispersive X-ray spectroscopy (EDS). An X-ray photoelectron spectroscopy (XPS) (Thermo escalab 250Xi) was utilized to analyze the bonding nature of $Bi_{0.5}Sb_{1.5}Te_3$ films. For the quantitative analysis of the different elements, five or more different regions of each sample were analyzed. In-plane electrical conductivity (σ) and Seebeck coefficient (S) were simultaneously measured on thin films deposited on 5 mm × 15 mm × 0.38 mm substrates by ZEM-3 (Ulvac Riko, Inc.). Cross-plane thermal conductivities were measured by a modified 3ω method at 300 K (Institute of Engineering Thermophysics, Chinese Academy of Sciences).

Contact resistance is measured by a four probe method using ZEM-3 (Ulvac Riko, Inc.). The detail is shown in Figure 1.

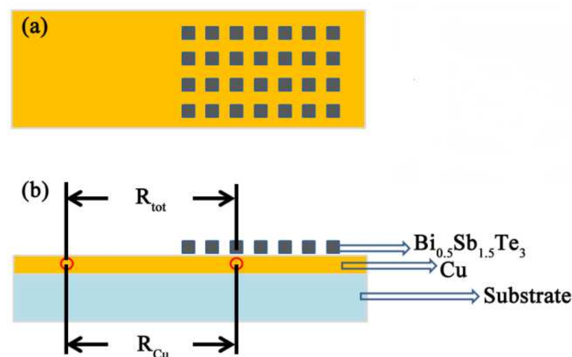

Figure 1 (a) Surface and (b) cross sectional view of experimental system. The contact resistance can be calculated by $R_{tot} = R_{Cu} + R_{Bi0.5Sb1.5Te3} + R_c$, where R_{tot}, R_{Cu}, $R_{Bi0.5Sb1.5Te3}$ and R_c are total resistace, resistance of copper, resistance of $Bi_{0.5}Sb_{1.5}Te_3$ and contact resistance.

RESULTS AND DISCUSSION

The metal-semiconductor interfacial structure is optimized by controlling the orientation of thermoelectric materials, achieving a maximum heat-flux pumping capability of 138 W cm^{-2} at T_c=300 K and a corresponding temperature difference of 6 K. The detail influential factors will be discussed in the following sections.

Calculation of Interfacial Lattice Mismatch

Table 1 Lattice mismatch between $Bi_{0.5}Sb_{1.5}Te_3$ and the Cu electrode

Cu	$Bi_{0.5}Sb_{1.5}Te_3$				Lattice mismatch / %
Lattice constant / Å	h	k	l	Lattice constant / Å	$\lvert\Delta a/a_{substrate}\rvert$
	0	1	5	3.1713	51.9
2.0880	1	1	0	2.1397	2.4
	0	0	15	2.0327	2.6

As mentioned above, the lattice mismatch plays an important role in thermoelectric devices. It allows for strain between the layers, which induces crystallographic defects,

Physical Chemistry Chemical Physics Accepted Manuscript

therefore generating greater resistance to the transportation of carriers or phonons, or macroscopic defects, such as buckling, cracking, and delamination[26]. The lattice mismatch $\Delta a/a_{\text{substrate}}$ is expressed by[27]:

$$\frac{\Delta a}{a_{substrate}} = \frac{a - a_{substrate}}{a_{substrate}} \times 100\% \tag{2}$$

where $a_{\text{substrate}}$ is the lattice constant of substrate. When the lattice mismatch $|\Delta a/a_{\text{substrate}}|$ is less than 5%, the two layers are completely coherent[28]. As shown in Table 1 (pattern JCPDS 49-1713 and JCPDS 04-0836), a lattice mismatch $|\Delta a/a_{\text{substrate}}| = 2.4\%$ is obtained. This indicates that the completely coherent structure of (110) oriented $Bi_{0.5}Sb_{1.5}Te_3$ on the Cu electrode may cause the enhanced adhesion of the metal-semiconductor structure and lead to a lower contact resistance. Hence, the (110) oriented thin film is the best choice for reducing contact resistance between the thermoelectric material and the Cu electrode.

Fabrication of (110) Oriented Thin Films

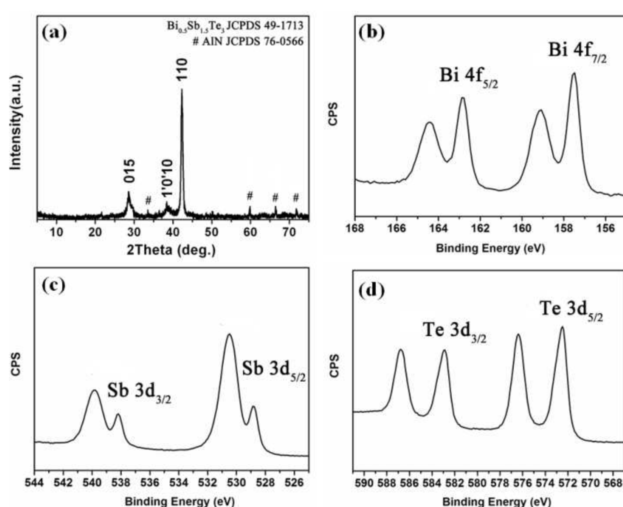

Figure 2 (a)XRD pattern of $Bi_{0.5}Sb_{1.5}Te_3$ films fabricated at 100 °C. XPS spectra of $Bi_{0.5}Sb_{1.5}Te_3$ flakes: (b) Bi 4f, (c) Sb 3d and (d) Te 3d.

Physical Chemistry Chemical Physics Accepted Manuscript

Physical Chemistry Chemical Physics Accepted Manuscript

Hierarchical $Bi_{0.5}Sb_{1.5}Te_3$ thin film was successfully prepared on a Cu thin film with a substrate temperature of 100 °C, a working pressure of 1.0 Pa and a sputtering power of 30 W. The XRD pattern in Figure 2 shows that the pattern is composed of peaks of $Bi_{0.5}Sb_{1.5}Te_3$ (JCPDS 49-1713, a = 4.284 Å, c = 30.524 Å), and marked peaks belong to the pattern of substrate AlN (JCPDS 76-0655). Compared with the standard pattern of $Bi_{0.5}Sb_{1.5}Te_3$, the pattern in Figure 2 demonstrates that the crystalline $Bi_{0.5}Sb_{1.5}Te_3$ is highly oriented in the (110) direction and weakly oriented in the (015) direction. The full width at half maximum of the (110) peak and the (015) peak are different, which indicates that the average grain size in the (110) orientation is much larger than that in the (015) orientation. The above results allow us to propose a hierarchical structure of the $Bi_{0.5}Sb_{1.5}Te_3$ films with a main direction and many small branches.

Figure 1(b), (c) and (d) show the XPS results of $Bi_{0.5}Sb_{1.5}Te_3$ films obtained at 100 °C. The Bi:Sb:Te atomic ratio were obtained as 0.50:1.51:2.99. The Bi $4f_{5/2}$ and Bi $4f_{7/2}$ peaks, Sb $d_{3/2}$ and $3d_{5/2}$, Te $3d_{3/2}$ and $3d_{5/2}$ were located at around 162.7 and 157.2 eV, 538.2 and 528.7 eV, 582.3 and 572.1 eV, respectively. Thus, it well reveals the proper character of $Bi_{0.5}Sb_{1.5}Te_3$. All the peaks had shoulders at higher binding energy, which indicated surface oxidation[29, 30]. From these XPS results, we speculate the $Bi_{0.5}Sb_{1.5}Te_3$ interface protection plays an important role in thermoelectric technology.

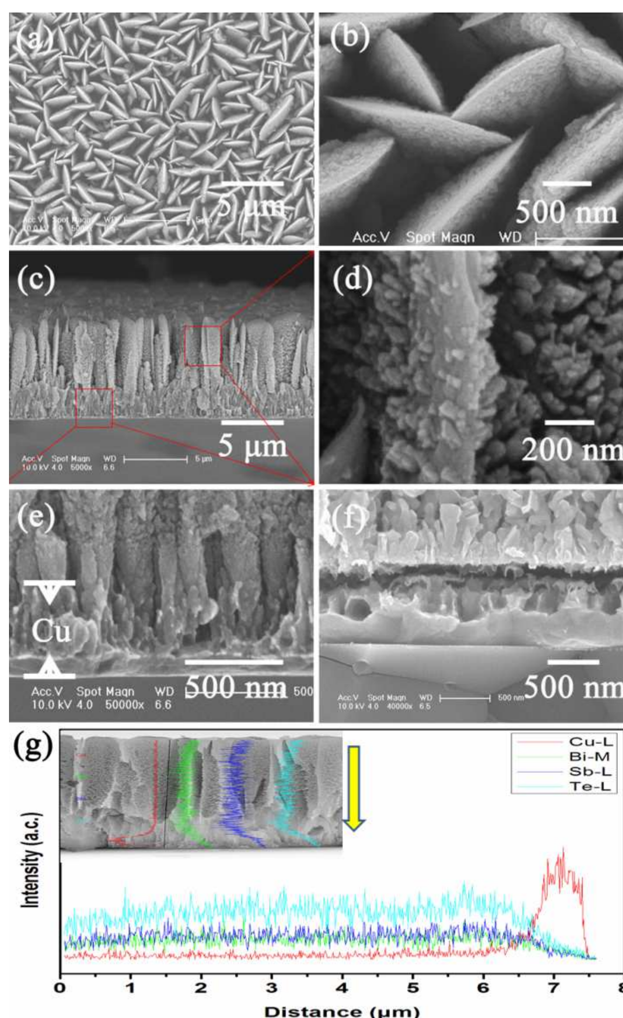

Figure 3 Surface (a, b) and cross-sectional view (c, d, e) of $Bi_{0.5}Sb_{1.5}Te_3$ film fabricated at 100 °C, and cross-sectional view (f) of ordinary thin film. The (110) oriented thin film closely connects to the Cu thin film without any obvious interfaces, while the ordinary thin film connects to Cu thin film with a crack. (g) SEM image of cross-sectional $Bi_{0.5}Sb_{1.5}Te_3$ and Cu EDS line scan profiles show the element distribution across the interface. The scan direction is marked by the yellow arrow.

The crystal structure was confirmed by scanning electron microscopy. Figure 3 shows the surface morphologies and the cross-sectional views of the $Bi_{0.5}Sb_{1.5}Te_3$ thin film, which was analyzed by field emission scanning electron microscopy (FE-SEM) equipped with EDS. The products usually exhibit cactus like shapes with an average size

Physical Chemistry Chemical Physics Accepted Manuscript

of 5.6 μm in length, 2.0 μm in width and 220 nm in thickness. From Figure 3a and 3b, the top view of the cactus like flakes can be easily observed. The flakes have many thorn like grains (about 50 nm) growing in the same direction. Figure 4a displays the TEM images of the $Bi_{0.5}Sb_{1.5}Te_3$ flakes. The HRTEM image shown in Figure 4b and 4c correlates with the d value of the (110) and (015) planes, where a lattice spacing of 0.21 nm and 0.32 nm were indexed. From Figure 4b and 4c, it is concluded that the flake has a main body in the (110) direction and branches in the (015) orientation.

In Figure 3c and 3d, dense columns (thickness of 2.0 μm, diameter from 100 nm to 300 nm) can be observed at the bottom and cactus like flakes can be observed at the top. This implies that the crystals are in a hierarchical structure and grow in a specific process. The thin film is continuous from bottom to top, and there is no layering and no separation between the $Bi_{0.5}Sb_{1.5}Te_3$ and the Cu thin film. Compared with the ordinary thin film on the Cu (Figure 3e and 3f) (110) oriented and Cu thin films, they are closely linked together without any obvious interfaces. However, the ordinary thin film connects to the Cu thin film with the presence of a crack. This is because of a mismatch of the coefficient of thermal expansion (CTE) between Bi_2Te_3 and the metal[31]. Figure 3(g) is a SEM image of a cross-sectional $Bi_{0.5}Sb_{1.5}Te_3$ film linked with a Cu layer. The EDS Cu L, Bi M, Sb L and Te L line scan profiles demonstrates that the Cu diffuses into the $Bi_{0.5}Sb_{1.5}Te_3$ layer (at approximately 400 nm away from the interface), which should be too thin to affect the performance of the device. The results of the EDS confirm that the products have a similar Bi:Sb:Te atomic ratio of ~ 0.5:1.5:3. The specific structure may be induced by the Cu film, which prompts us to investigate the effect of the substrate.

Physical Chemistry Chemical Physics Accepted Manuscript

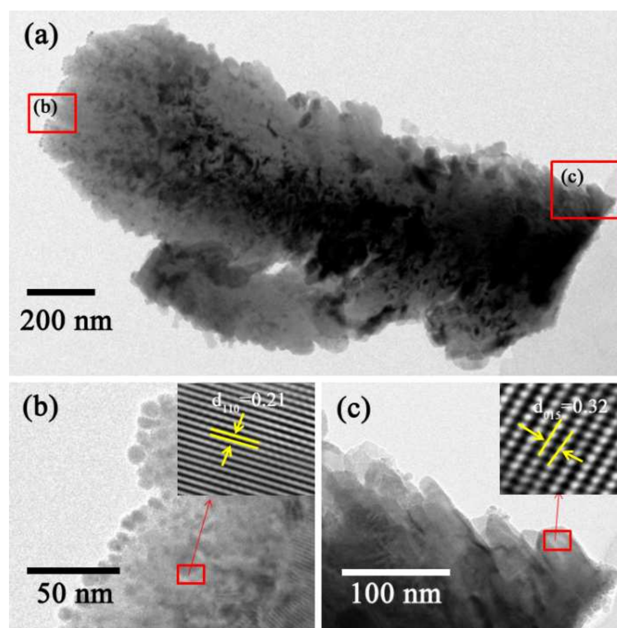

Figure 4 (a–c) TEM images of $Bi_{0.5}Sb_{1.5}Te_3$ flakes, and insets in (b) and (c) show the HRTEM images of (b) and (c) respectively.

A substrate dependent experiment was conducted on PI (κ ≈ 0.2 W/ (m K)), AlN (κ ≈ 130 W/ (m K)) and the unpolished AlN substrate as shown in Figure 5. Although there is no column like structure at the bottom, the products are quite similar to the flakes fabricated on the Cu thin film surface. This indicates that the substrate is not a critical factor for $Bi_{0.5}Sb_{1.5}Te_3$ growth with a (110) oriented direction. However, the height of the flakes and the size of (015) oriented side grains are quite different from the products on Cu thin film surface. This can be attributed to the following aspects: Firstly, the height of the flakes is related to the type of substrate. Secondly, the thickness of the column like grains and the size of the (015) oriented side grains are induced by the interfacial structure.

Physical Chemistry Chemical Physics Accepted Manuscript

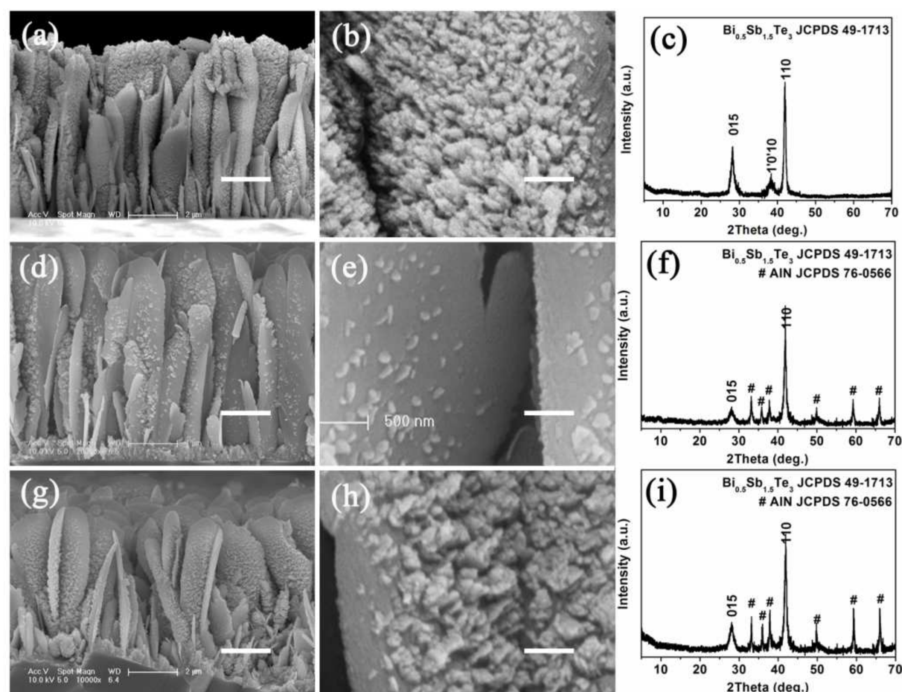

Figure 5 SEM images of nanocrystals deposited on different substrate: (a, b) PI, (d, e) polished AlN, and (g, h) unpolished AlN. XRD patterns of $Bi_{0.5}Sb_{1.5}Te_3$ on: (c) PI, (f) polished AlN, and (i) unpolished AlN.

Structure of the (015) Oriented branches

To confirm that the hierarchical structure is controllable, the deposition temperature was increased to 200 °C on the Cu thin film surface as shown in Figure 6. The XRD pattern in Figure 7 is similar with the pattern in Figure 2. Compared with the XRD pattern in Figure 2, the peak intensity in Figure 7 demonstrates that the main body flakes in the (110) direction decrease and the branch grains in the (015) direction increase.

Physical Chemistry Chemical Physics Accepted Manuscript

Physical Chemistry Chemical Physics Accepted Manuscript

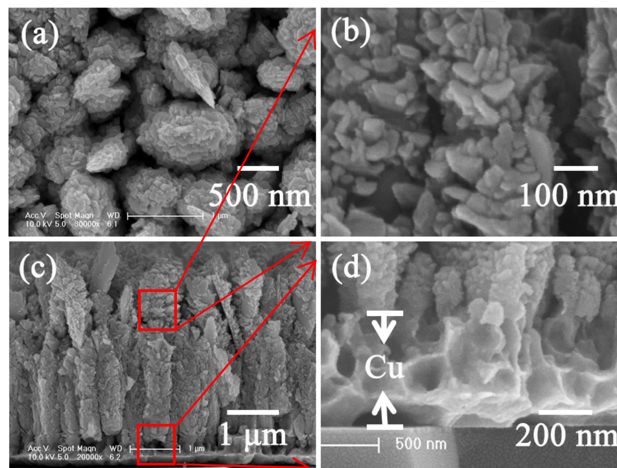

Figure 6 SEM photograph of the (110) oriented hierarchical $Bi_{0.5}Sb_{1.5}Te_3$ films fabricated at 200 °C: (a) surface view; (b, c, d) cross-sectional view.

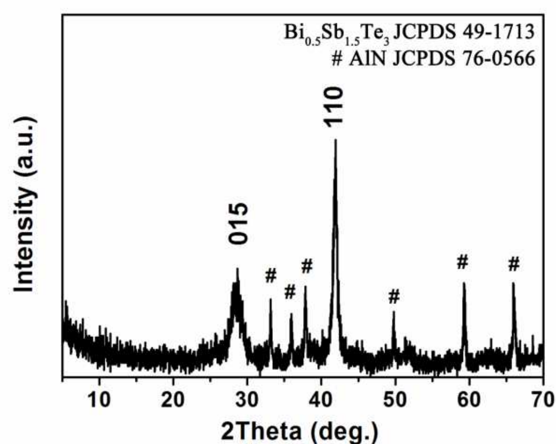

Figure 7 XRD pattern of the (110) oriented hierarchical $Bi_{0.5}Sb_{1.5}Te_3$ films fabricated at 200 °C.

Furthermore, Figure 6 shows the surface morphologies and the cross-sectional views of $Bi_{0.5}Sb_{1.5}Te_3$ thin films fabricated at 200 °C. The products have an average size of 3.4 μm in length, 610 nm in width and 500 nm in thickness. The average grain size in the side face grows to 80 nm. The bottom column like structure has not changed, which is in accord with our substrate induced results. Most crystals are independent at the top of the structure, which will affect the in plane transport properties and connection in the cross

plane.

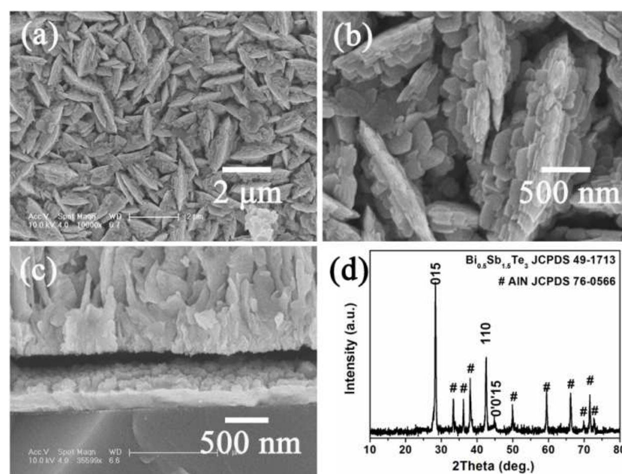

Figure 8 (110) oriented hierarchical $Bi_{0.5}Sb_{1.5}Te_3$ films fabricated at 300 °C: (a, b) SEM pictures of surface view, and (c) cross-sectional view; (d) XRD pattern.

When the deposition temperature is increased to 300 °C on the Cu thin film surface, the surface morphology (Figure 8a and 8b) demonstrates that the branches are composed of hexagonal slices with an average size of approximately 200 nm. Compared with the morphology of films at 100 °C and 200 °C, the (015) oriented crystals exhibit a flat surface and sharp edges with excellent crystallinity. It demonstrates that the high temperature is beneficial for the growth of (015) oriented thin films. From the cross-sectional view (Figure 8c), it can be clearly seen that there is an obvious separation between the $Bi_{0.5}Sb_{1.5}Te_3$ and the Cu thin film because of the coefficient of thermal expansion (CTE) mismatch between the Bi_2Te_3 and the metal. This can be confirmed by the significantly increased intensity of the (015) peak as shown in Figure 8d. Compared with the film with the preferential growth in the (110) plane, the (015) peak is higher than the (110) peak. This indicates that the lattice mismatch is much higher than that of the

Physical Chemistry Chemical Physics Accepted Manuscript

Physical Chemistry Chemical Physics Accepted Manuscript

(110) oriented thin film, leading to breakage between the thermoelectric materials and the metal. For this reason, this work focuses on the (110) oriented thin film deposited at 100 °C and 200 °C. To further understand the bottom up growth of the hierarchical $Bi_{0.5}Sb_{1.5}Te_3$ thin films, a time dependent experiment is conducted on Cu thin film substrate, at 100 °C for a period of 40, 80, 120 or 180 min.

Evolution of Morphology and Growth Mechanisms

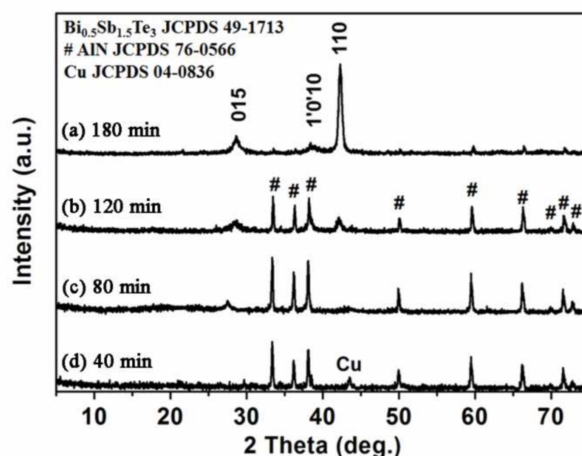

Figure 9 XRD patterns of $Bi_{0.5}Sb_{1.5}Te_3$ films with different deposition times: (a) 180 min, (b) 120 min, (c) 80 min, and (d) 40 min.

XRD data provide further information on the crystal growth process. The XRD patterns in Figure 9 show that the patterns are composed of the substrate AlN (JCPDS 76-0655), the Cu thin film (JCPDS 04-0836) and the $Bi_{0.5}Sb_{1.5}Te_3$ (JCPDS 49-1713, a = 4.284 Å, c = 30.524 Å). As shown in Figure 9, the characteristic diffraction peaks of $Bi_{0.5}Sb_{1.5}Te_3$ increase with the deposition time, which are well matched with the standard pattern of $Bi_{0.5}Sb_{1.5}Te_3$. The decreasing intensity of AlN and Cu also indicate the increasing thickness of the $Bi_{0.5}Sb_{1.5}Te_3$ thin films. Furthermore, the two peaks at the diffraction angles of 28.12° and 42.20° are at exactly the same position as the peaks from

Physical Chemistry Chemical Physics Accepted Manuscript

the diffracted $Bi_{0.5}Sb_{1.5}Te_3$ structures in the preferential (015) and (110) directions respectively, which increase with the increasing deposition time. The particularly high peak in Figure 9a reveals that the (110) direction is the main orientation of the thin film. Compared with the standard pattern of $Bi_{0.5}Sb_{1.5}Te_3$, the pattern in Figure 9a demonstrates that the crystalline $Bi_{0.5}Sb_{1.5}Te_3$ are highly oriented in the (110) direction and weakly oriented in the (015) direction.

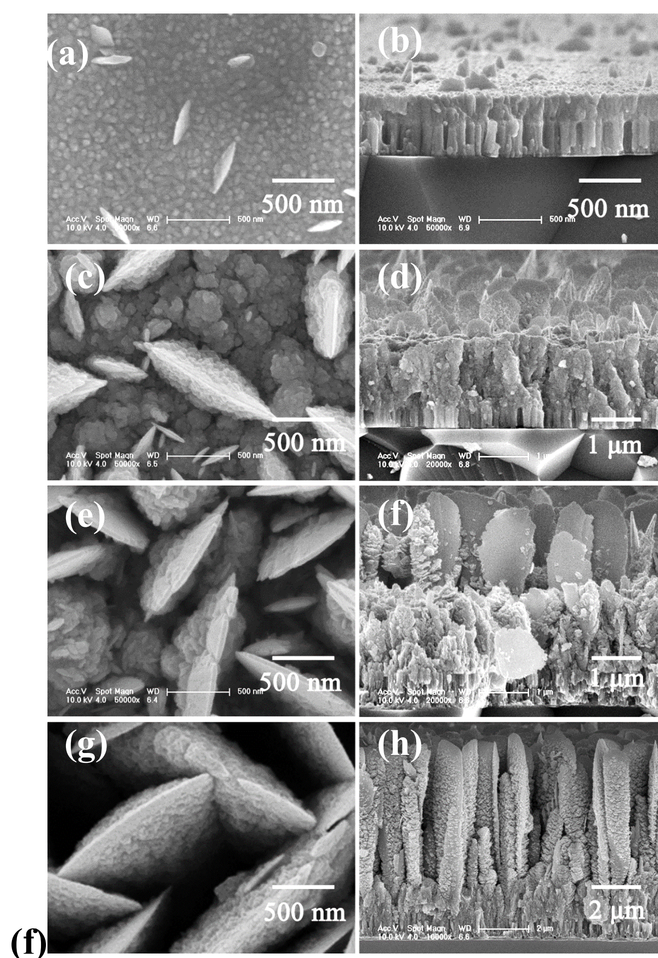

Figure 10 SEM images of the $Bi_{0.5}Sb_{1.5}Te_3$ nanocrystals fabricated by the magnetron method at 100 °C for various time intervals: (a, b) 40, (c, d) 80, (e, f) 120, and (g, h) 180 min.

According to the above discussion, the formation process of the hierarchical

Physical Chemistry Chemical Physics Accepted Manuscript

$Bi_{0.5}Sb_{1.5}Te_3$ nanostructures is proposed in Figure 10. It can be observes that the growth of the hierarchical flakes can be approximately described as a three-step process. In the first step, as shown in Figure 10a and 10b, small grains (~50 nm) accumulate on the Cu thin film surface. The surface of the nanograins is almost void of any (110) oriented flakes, which have barely, started to grow. Hence, the grains are too small to be detected in XRD patterns. Secondly, the density and size of the $Bi_{0.5}Sb_{1.5}Te_3$ flakes increase considerably (as compared to Figure 10a and 10b) after 80 min and 120 min of $Bi_{0.5}Sb_{1.5}Te_3$ growth (Figure 10c, 10d, 10e and 10f). Meanwhile, the thicknesses of the bottom columns increase. Also, the grains in the side face increase. The growth rate of the branches is faster than that of the (110) oriented main body. It is the reason that the (015) peak is higher than (110) peak at 80 min. Finally, this process continues for a period of over 180 min (see Figure 10g and 10h), when the nanoflakes join together and develop a substantial density of side grains, which are oriented in the (015) direction (corresponding to XRD patterns). In addition, the hierarchical flakes show a tendency of initially growing mostly in height; following this period of vertical growth, the width and volume of the nanoflakes tend to expand by radial growth and by developing a higher density of side (015) oriented grains. Although the detailed deposition mechanism of this phenomenon is not clear, the above results allow us to speculate a possible process to obtain hierarchical $Bi_{0.5}Sb_{1.5}Te_3$ flakes with different orientation (Figure 11).

The growth process of the films is based on the Volmer-Weber mode. In this steady-state regime, the island density (N) should increase with an increase in the deposition rate (F) and decrease with the surface diffusion coefficient (D). It has the qualitative form $N \propto F^p/D^q$ (the values of p and q are positive) [32, 33]. The deposition rate

(*F*) is related to the mechanism of magnetron sputtering. The main system for the magnetron sputtering technique consists of a pair of planar electrodes (the anode-substrate, the cathode-target). The two electrodes are located inside a low pressure vacuum deposition chamber. This is a chamber filled with the sputtering gas, which is usually an inert gas such as Argon (Ar). Once negative voltage is applied to the target surface, any existing Ar positive ions will accelerate towards the cathode. When the Ar position ions fall on the cathode, a small stream of atoms or clusters of atoms will eject from the cathode material. A small portion of atom will impact on the substrate, leading to the formation of a thin film. Therefore, the deposition rate increases with an increase in the working power and decrease working pressure.

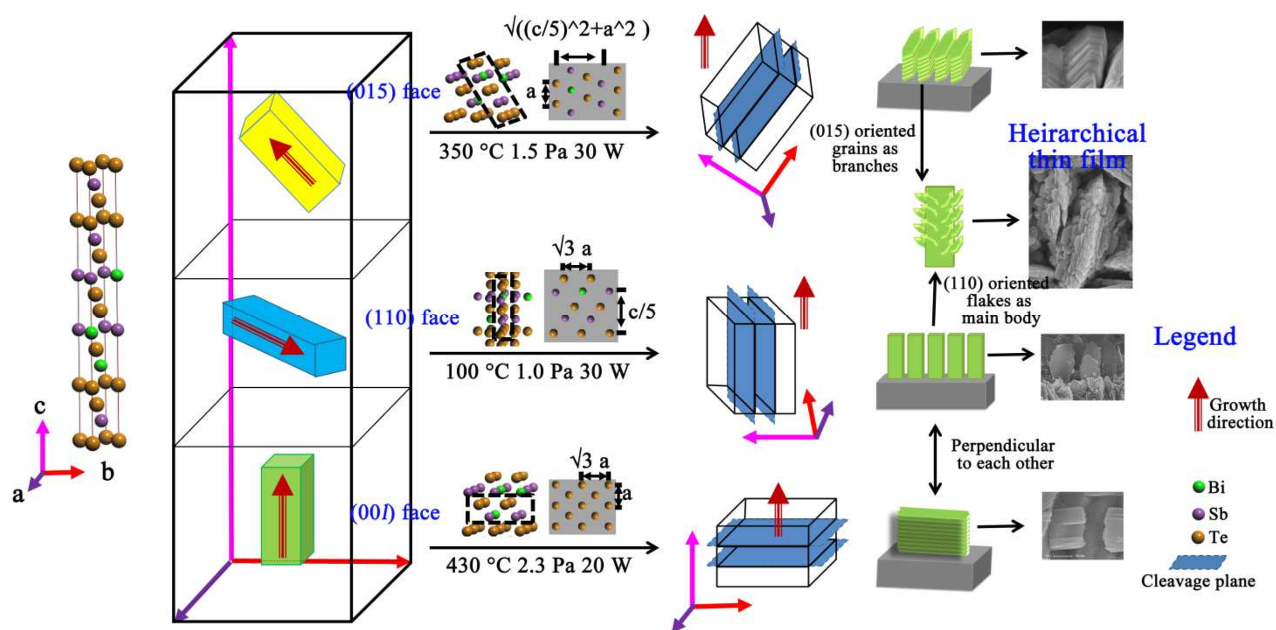

Figure 11 Schematic illustrations of the $Bi_{0.5}Sb_{1.5}Te_3$ thin films.

Furthermore, the surface diffusion coefficient (*D*) is related to the site-to-site

Physical Chemistry Chemical Physics Accepted Manuscript

hopping rate of an adatom, k_s, by $D=a^2 k_s$, where a is the effective hopping distance between sites, and $k_s \propto exp\{-V_s/k_BT\}$, where V_s is the potential-energy barrier from site to site, T is the substrate temperature, and k_B is the Boltzmann constant[34]. If the effective hopping distance (a) is fixed, the substrate temperature determines the surface diffusion coefficient (D). In addition, the atom layers of Bi_2Te_3 and similar compounds have a -Te(1) - Bi(Sb)-Te(2)-Bi(Sb)-Te(1) structure[6, 35]. Here, Te has two different coordination environments in the crystal structure. The two adjacent Te(1) layers along the c-axis interact with each other by Vander-Waals forces, which is not strong enough to fix an atom on the smooth surface. Therefore, a Bi_2Te_3 based crystal has an interface that is perpendicular to the c axis, regardless of the crystal growth in any direction (shown in Figure 11). The distance between the Te(1) and Te(1) layers (the first row in Figure 11) in the (110) direction is smaller than those in the (015) and (00*l*) directions, resulting in smaller island size and a larger island density. So the (110) oriented thin film is fabricated at a low working pressure, high working power and a low substrate temperature. Otherwise, the (00*l*) oriented thin film is obtained[36].

Transport properties and Interface Dependent Performance of Device

The in-plane transport properties of the $Bi_{0.5}Sb_{1.5}Te_3$ thin film as a function of temperature have been investigated using the four probes method in a commercially available ZEM-3 system and is demonstrated in Figure 12. Figure 12a shows that the electrical conductivity decreases with increasing temperature, indicating a metallic like behavior[37]. The value of electrical conductivity reaches 4.5×10^4 S m^{-1}, 6.6×10^4 S m^{-1} and 5.2×10^4 S m^{-1} at 305 K, while the hierarchical thin film has electrical conductivities above 4.0×10^4 S m^{-1} for the whole temperature range. The temperature-dependent

Physical Chemistry Chemical Physics Accepted Manuscript

Seebeck coefficient of the thin film is shown in Figure 12b. The Seebeck coefficient of hierarchical thin film was ~ 150 μV K^{-1} at room temperature and decreases to 110 μV K^{-1} with the increased deposition temperature. The power factor for the hierarchical $Bi_{0.5}Sb_{1.5}Te_3$ thin film is shown in Figure 12c. The maximum values of the power factor are 10.3×10^{-4} W m^{-1} K^{-2}, 12×10^{-4} W m^{-1} K^{-2} and 6.6×10^{-4} W m^{-1} K^{-2} at 100 °C, 200 °C and 300 °C reapectively, which is similar to the results of other researchers[38, 39].

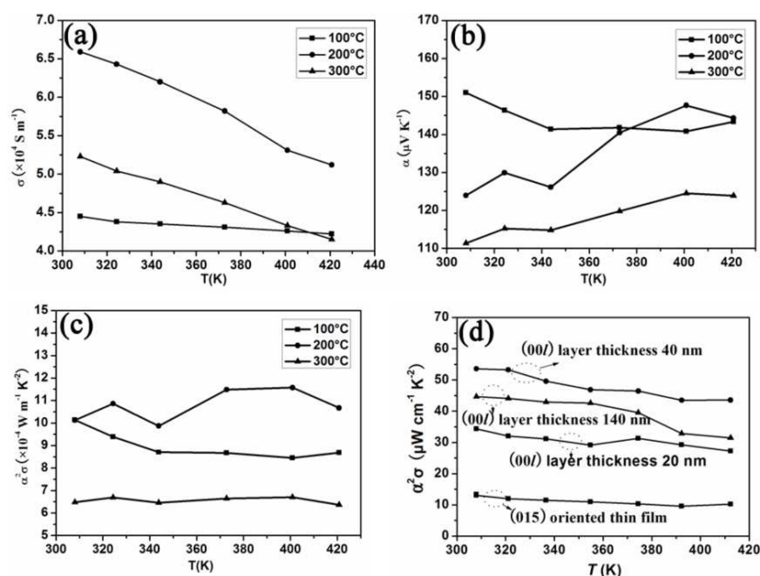

Figure 12 In plane transport properties of the hierarchical $Bi_{0.5}Sb_{1.5}Te_3$ film at different deposition temperatures: (a) electrical conductivity, (b) Seebeck coefficient and (c) power factor; (d) power factor of (00*l*) and (015) oriented thin film. The power factor of the (00*l*) oriented thin film is controllable by changing the layer thickness[36].

Previous reports calculated the out plane ZT from the in-plane electrical conductivity and Seebeck coefficient for the same thin film, which reveals that the out plane electrical conductivity and Seebeck coefficient to be approxiately 12–15% higher than the in plane properties[40]. Thus, the out plane power factor can reach 18.3×10^{-4} W m^{-1} K^{-2}. The out plane thermal conductivity at room temperature is approximately 1.0 W

Physical Chemistry Chemical Physics Accepted Manuscript

m^{-1} K^{-1} for the hierarchical $Bi_{0.5}Sb_{1.5}Te_3$ thin film with (110) orientation. The out plane ZT may reach at the value greater than 0.73 at a temperature of 400 K.

Table 2 Properties of the cross plane values of thin film material.

Properties	n-$Bi_2Te_{2.7}Se_{0.3}$ [41]	p-$Bi_{0.5}Sb_{1.5}Te_3$
Seebeck coefficient (α)	-196 μV K^{-1}	173 μV K^{-1}
Electrical conductivity (σ)	6.5×10^4 S m^{-1}	6.0×10^4 S m^{-1}
Thermal conductivity (k)	0.91 W m^{-1} K^{-1}	1.0 W m^{-1} K^{-1}

The heat-flux pumping capability of TEC can be achieved by Eq. 1. The results calculated are based on a (110) oriented $Bi_{0.5}Sb_{1.5}Te_3$ thermoelectric thin films, which has a typical out plane Seebeck coefficient of 173×10^{-6} V/K and electrical conductivity of 6.0×10^4 S m^{-1}. The thickness of the hierarchical thin film is 10 μm and the thermal conductivity is 1.0 W m^{-1} K^{-1}. The values of the thin film material properties are shown in Table 2**.** The TEC module has 98 thermocouples with a thermoelement cross-sectional area of 1 mm × 1 mm with a contact resistance 1.0×10^{-3} Ω (measured by four probe method in Figure 1). The contact resistivity is given by $r_c = R_c \cdot A^3$, which is 1.0×10^{-9} Ω m^2. A maximum heat-flux pumping capability of 138 W cm^{-2} can be obtained for T_c=400 K and the corresponding temperature difference is 6 K, which is similar to the result in our previous work[41]. The enhanced refrigeration capability is achieved by the effects of low contact resistance and a high ZT value because of the reduced interfacial lattice mismatching and the optimized crystal structure.

CONCLUSION

Physical Chemistry Chemical Physics Accepted Manuscript

In summary, high refrigeration performance is obtained by controlling the metal-semiconductor interface and the structure of the (110) oriented hierarchical $Bi_{0.5}Sb_{1.5}Te_3$ flakes, which have been successfully fabricated by the magnetron sputtering method. The hierarchical flakes are 5.6 μm in length, 2.0 μm in width and 220 nm in thickness when prepared at a temperature of 100 °C, and 3.4 μm in length, 610 nm in width and 500 nm in thickness at 200 °C. The average grain size in the side face grows from 50 nm to 80 nm with the increasing in the deposition temperature. The growth mechanism implies that the deposition rate increases with increasing working power and decreasing working pressure, and the substrate temperature determines the surface diffusion coefficient. Furthermore, the lattice structure of the Cu electrode is well matched to that of the hierarchical thin film at a high depositing rate and a low temperature. The lattice mismatching is lower than 2.4%. This is achieved by controlling the metal-semiconductor interfacial effect, which results in a low contact resistance of 1.0 $\times 10^{-9}$ Ω m^2. The measured out plane thermal conductivity is about 1.0 W m^{-1} K^{-1} at room temperature. Based on the properties of hierarchical (110) oriented $Bi_{0.5}Sb_{1.5}Te_3$ material, a maximum heat-flux pumping capability of 138 W cm^{-2} is calculated for T_c=400 K in a 98 thermocouples TEC module and the corresponding temperature difference is 6 K. Our work establishes that satisfactory lattice matching can reduce the interfacial dislocation density and defects. This indicates that controlling the structure on electrode is an efficient method to reduce contact resistance. This study represents an advancement in the understanding of the cross-plane performance of thin film devices.

ACKNOWLEDGMENTS

Physical Chemistry Chemical Physics Accepted Manuscript

Physical Chemistry Chemical Physics Accepted Manuscript

The work was supported by the State Key Development Program for Basic Research of China (Grant No.2012CB933200), National Natural Science Foundation of China (No. 51172008 and 51002006), National Natural Science Fund Innovation Group (No. 51221163), Research Fund for Doctor Station Sponsored by the Ministry of Education of China (20111102110035) and the Fundamental Research Funds for the Central Universities.

REFERENCES

(1) H. J. Goldsmid and R. W.Douglas, *Thermoelectric Refrigeration*, 3rd ed. Plenum: New York, 1964.

(2) T. C. Harman, P. J. Taylor, M. P. Walsh and B. E. LaForge, Quantum Dot Superlattice Thermoelectric Materials and Devices. *science* **2002**, *297*, 2231-2232.

(3) D. M. Rowe, *CRC Handbook of Thermoelectrics*, CRC Press: Boca Raton, FL, 1995.

(4) M. W. Oh, J. H. Son, B. S. Kim, S. D. Park, B. K. Min and H. W. Lee, Antisite Defects in N-type $Bi_2(Te,Se)_3$: Experimental and Theoretical Studies. *J. Appl. Phys.* **2014**, *115*, 133706.

(5) J. S. Son, H. Zhang, J. Jang, B. Poudel, A. Waring, L. Nally and D. V. Talapin, All-Inorganic Nanocrystals as a Glue for BiSbTe Grains: Design of Interfaces in Mesostructured Thermoelectric Materials. *Angew. Chem., Int. Ed.* **2014**, *53*,7466-7470.

(6) L. P. Hu, T. J. Zhu, Y. G. Wang, H. H. Xie, Z. J. Xu and X. B. Zhao, Shifting up the Optimum Figure of Merit of P-type Bismuth Telluride-based Thermoelectric Materials for Power Generation by Suppressing Intrinsic Conduction. *NPG Asia Mater.* **2014**, *6*, e88

Physical Chemistry Chemical Physics Accepted Manuscript

(7) K. Kato, Y. Hatasako, M. Uchino, Y. Nakata, Y. Suzuki, T. Hayakawa, C. Adachi, and K. Miyazaki, Flexible Porous Bismuth Telluride Thin Films with Enhanced Figure of Merit using Micro-Phase Separation of Block Copolymer. *Adv. Mater. Interfaces* **2014**, *1*, 1300015.

(8) Z. Cao, E. Koukharenko, M. J. Tudor, R. N. Torah and S. P. Beeby, Screen Printed Flexible Bi_2Te_3-Sb_2Te_3 Based Thermoelectric Generator. *J. Phys.: Conf. Ser.* **2013**, *476*, 012031.

(9) L. Li, Y. W. Yang, X. H. Huang, G. H. Li and L. D. Zhang, Pulsed Electrodeposition of Single-crystalline Bi_2Te_3 Nanowire Arrays. *Nat. Nanotechnol.* **2006**, *17*, 1706–1712.

(10) D. Koumoulis, B. Leung, T. C. Chasapis, R. Taylor, J. D. King, M. G. Kanatzidis and L. S. Bouchard, Understanding Bulk Defects in Topological Insulators from Nuclear-Spin Interactions. *Adv. Funct. Mater.* **2014**, *24*, 1519–1528.

(11) H. Cao, R. Venkatasubramanian, C. Liu, J. Pierce, H. Yang, M. Z. Hasan, Y. Wu and Y. P. Chen, Topological Insulator Bi_2Te_3 Films Synthesized by Metal Organic Chemical Vapor Deposition. *Appl. Phys. Lett.* **2012**, *101*, 162104.

(12) S. E. Harrison, S. Li, Y. Huo, B. Zhou, Y. L. Chen and J. S. Harris, Two-step Growth of High Quality Bi_2Te_3 Thin Films on Al_2O_3 (0001) by Molecular Beam Epitaxy. *Appl. Phys. Lett.* **2013**, *102*, 171906.

(13) X. H. Li, E. Koukharenko, I. S. Nandhakumar, J. Tudor, S. P. Beeby and N. M. White, High Density P-type $Bi_{0.5}Sb_{1.5}Te_3$ Nanowires by Electrochemical Templating Through Ion-track Lithography. *Phys. Chem. Chem. Phys.* **2009**, *11*, 3584–3590

(14) D. Zhao, M. Zuo and H. Geng, Enhanced Thermoelectric Performance of Ga-added $Bi_{0.5}Sb_{1.5}Te_3$ Films by Flash Evaporation. *Intermetallics* **2012**, *31*, 321-324.

(15) S. Yoon, J. Y. Cho, H. Koo, S. H. Bae, S. Ahn, G. R. Kim and J. S. Kim, Thermoelectric Properties of *n*-Type Bi_2Te_3/$PbSe_{0.5}Te_{0.5}$ Segmented Thermoelectric Material. *J. Electron. Mater.* **2014**, *43*, 414-418.

(16) Y. Zhang,; L. P. Hu, T. J. Zhu, J. Xie and X. B. Zhao, High Yield Bi_2Te_3 Single Crystal Nanosheets with Uniform Morphology via a Solvothermal Synthesis. *Cryst. Growth Des.* **2013**, *13*, 645−651.

(17) L. D. Zhao, S. H. Lo, Y. S. Zhang, H. Sun, G. J. Tan, C. Uher, C. W. Vinayak, P. D.Mercouri and G. Kanatzidis, Ultralow Thermal Conductivity and High Thermoelectric Figure of Merit in SnSe Crystals. *Nature* **2014**, *508*, 373-377.

(18) X. Yan, B. Poudel, Y. Ma, W. S. Liu, G. Joshi, H. Wang, Y. C. Lan, D. Z.Wang, G. Chen and Z. F. Ren, Experimental Studies on Anisotropic Thermoelectric Properties and Structures of n-Type $Bi_2Te_{2.7}Se_{0.3}$. *Nano Lett.* **2010**, *10*, 3373–3378.

(19) K. Xiong, W. C. Wang, H. N. Alshareef, R. P. Gupta, J. B. White, B. E. Gnade and K. Cho, Electronic Structures and Stability of Ni/Bi_2Te_3 and Co/Bi_2Te_3 Interfaces. *J. Phys. D: Appl. Phys.* **2010**, *43*, 115303.

(20) Y. C. Lan, D. Z. Wang, G. Chen and Z. F. Ren, Diffusion of Nickel and Tin in P-type $(Bi, Sb)_2Te_3$ and N-type $Bi_2(Te, Se)_3$ Thermoelectric Materials. *Appl. Phys. Lett.* **2008**, *92*, 101910.

(21) O. D. Iyore, T. H. Lee, R. P. Gupta, J. B. White, H. N. Alshareef, M. J. Kim and B.E. Gnade, Interface Characterization of Nickel Contacts to Bulk Bismuth Tellurium Selenide. *Surf. Interface Anal.* **2009**, *41*, 440–444.

(22) Y. Y. Li, G. Wang, X. G. Zhu, M. H. Liu, C. Ye, X. Chen, Y. Y. Wang, K. He, L. L. Wang, X. C. Ma, H. J. Zhang, X. Dai, Z. Fang, X. C. Xie, Y. Liu, X. L. Qi, J. F. Jia, S. C.

Physical Chemistry Chemical Physics Accepted Manuscript

Zhang and Q. K. Xue, Intrinsic Topological Insulator Bi_2Te_3 Thin Films on Si and Their Thickness Limit. *Adv. Mater.* **2010**, *22*, 4002–4007.

(23) L. W. Silva and M. Kaviany, Micro-thermoelectric Cooler: Interfacial Effects on Thermal and Electrical Transport. *Int. J. Heat Mass Transfer* **2004**, *47*, 2417-2435.

(24) J. P. Fleurial, A. Borshchevsky, M.A. Ryan, W. Phillips, E. Kolawa, T. Kacisch and R. Ewell, Thermoelectric Microcoolers for Thermal Management Applications. *16th Int. Conf. Thermoelectr.* **1997**, 641-645.

(25) M. R. Miguel, C. C. Olga and M. G. Marisol, Electrical Contact Resistances of Thermoelectric Thin Films Measured by Kelvin Probe Microscopy. *Appl. Phys. Lett.* **2013**, *103*, 183905.

(26) A. Moridi, H. H. Ruan, L. C. Zhang and M. Liu, Residual Stresses in Thin Film Systems: Effects of Lattice Mismatch, Thermal Mismatch and Interface Dislocations. *Int. J. Solids Struct.* **2013**, *50*, 3562–3569.

(27) M. Boucenna, N. Bouarissa and Mezrag, F. Composition and Lattice Mismatch Dependent Dielectric Constants and Optical Phonon Modes of $InAs_{1-x-y}Sb_xP_y$ Quaternary Alloys. *Infrared Phys. Technol.* **2014**, *67*, 318-322.

(28) J. Pan, J. M. Tong and M. B. Tian, Basic of Materials Science; Tsinghua University Press, 2004.

(29) K. T. Kim, S. Y. Choi, E. H. Shin, K. S. Moon, H. Y. Koo, G. Lee, G. H. Ha, The Influence of CNTs on the Thermoelectric Properties of a CNT/Bi_2Te_3 Composite, *Carbon* **2013**, *52*, 541-549.

Physical Chemistry Chemical Physics Accepted Manuscript

Physical Chemistry Chemical Physics Accepted Manuscript

(30) M. R. Dirmyer, J. Martin, G. S. Nolas, A. Sen, and J. V. Badding, Thermal and Electrical Conductivity of Size-Tuned Bismuth Telluride Nanoparticles, *Small* **2009**, *5*, 933-937.

(31) W. P. Lin, D. E. Wesolowski and C. C. Lee, Barrier/bonding Layers on Bismuth Telluride (Bi_2Te_3) for High Temperature Thermoelectric Modules. *J. Mater. Sci: Mater. Electron.* **2011**, *22*, 1313–1320.

(32) Y. W. Mo, J. Kleiner, M. B. Webb and M. G. Lagally, Activation Energy for Surface Diffusion of Si on Si(001):A Scanning-Tunneling-Microscopy Study. *Phys. Rev. Lett.* **1991**, *66*, 1998-2002.

(33) A. Pimpinelli, J. Villain and D. E. Wolf, Surface Diifusion and Island Density. *Phys. Rev. Lett.* **1992**, *69*, 985.

(34) Z. Y. Zhang and M. G. Lagally, Atomistic Processes in the Early Stages of Thin-Film Growth. *Science* **1997**, *276*, 377-383.

(35) L. L. Guo, A. Aglan, H. Y. Quan, J. J. Sun, C. L. Tang, J. H. Song, G. Szulczewski and H.-T. Wang, Selective Adsorption of Bismuth Telluride Nanoplatelets through Electrostatic Attraction. *Phys. Chem. Chem. Phys.* **2014**, *16*, 11297-11302

(36) L. L. Cao, Y. Wang, Y. Deng, H. L. Gao, B. W. Luo and W. Zhu, Facile Synthesis of Preferential $Bi_{0.5}Sb_{1.5}Te_{3.0}$ Nanolayered Thin Films with High Power Factor by the Controllable Layer Thickness. *J. Nanopart. Res.* **2013**, *15*, 2088.

(37) F. R. Yu, J. J. Zhang, D. L. Yu, J. L. He, Z. Y. Liu, B. Xu and Y. J. Tian, Enhanced Thermoelectric Figure of Merit in Nanocrystalline Bi_2Te_3 Bulk. *J. Appl. Phys.* **2009**, *105*, 094303.

(38) A. J. Naylor, E. Koukharenko, I. S. Nandhakumar and N. M. White, Surfactant-Mediated Electrodeposition of Bismuth Telluride Films and Its Effect on Microstructural Properties. *Langmuir* **2012**, *28*, 8296−8299.

(39) I. J. Yoo, Y. Song, D. C. Lim, N. V. Myung, K. H. Lee, M. Oh, D. Lee, Y. D. Kim, S. Kim, Y. H. Choa, J. Y. Lee, K. H. Lee and J. H. Lim, Thermoelectric Characteristics of Sb_2Te_3 Thin Films Formed via Surfactant-assisted Electrodeposition. *J. Mater. Chem. A* **2013**, *1*, 5430-5435.

(40) H. Choi, J. H. Baeck, T. H. Kim, J. Y. Song, S. W. Shin, H. H. Cho, D. H. Ko, J. S. Kim, K. H. Jeong and M. H. Cho, Synthesis of Self-ordered Sb_2Te_2 Films with Atomically Aligned Te Layers and the Effect of Phonon Scattering Modulation. *J. Mater. Chem. C* **2013**, *1*, 7043–7053.

(41) M. Tan, Y. Deng and Y. M. Hao, Improved Thermoelectric Performance of a Film Device Induced by Densely Columnar Cu Electrode. *Energy* **2014**, *70*, 143-148.

Physical Chemistry Chemical Physics Accepted Manuscript